

Unresolved CFD-DEM of sandstone-laden air flow in a clear channel

S.T.W.Kuruneru¹, E.Sauret¹, S.C. Saha¹ and Y.T. Gu¹

¹School of Chemistry, Physics & Mechanical Engineering, Queensland University of Technology, Brisbane, Queensland,4011, Australia

Abstract

An unresolved finite-volume and discrete-element method that is able to capture the interaction between the lagrangian particles and carrier fluid in a clear channel is investigated. A hybrid SIMPLE-PISO algorithm is used to achieve pressure-velocity coupling whilst concurrently achieving stable and faster numerical convergence. Although the unresolved method is applicable if the CFD mesh cell size is larger than DEM particle size, this preliminary study shows that the unresolved method produces similar results in the event the particle diameter vastly exceeds the mesh cell size. Quantitative analysis shows near identical results among all four CFD grids tested. The gas void fraction exchange fields becomes smooth as the CFD mesh cell size exceeds the DEM particle size. Good agreement is observed between the analytical and numerical pressure drop profiles.

Introduction

Multiphase flows and particulate suspensions are omnipresent in various natural and industrial systems. The development of a robust and accurate numerical model would be of significant importance in order to comprehend the mechanisms of multiphase transport (*i.e.* solid-solid, solid-liquid, liquid-gas) [15]. A solid understanding of the mechanisms of particle-fluid transport and particle deposition will permit engineers to better design engineering systems such as heat exchangers. A coupled numerical approach to study multiphase transport in clear or porous channels is rapidly gaining attention. Lakeh *et al.* [9] used Eulerian-Eulerian numerical approach to predict particle deposition on a blade surface of a turbomachinery. Specific regions are shown to exhibit high traces of particle deposits which affect the boundary layers and blade aerodynamics. Zhou [16] used the Eulerian-Eulerian approach to study gas-particle flows and coal combustion. A major observation is that the unified second-order moment (USM) (or two-phase Reynolds stress model) and $k-\varepsilon$ -kp two-phase turbulence models can reasonably predict particle-bubble turbulence. Instantaneous particle and gas streamlines for two-phase swirling flows was studied. Sauret and Hooman [13] used the Eulerian-Lagrangian approach to predict the location of particulate foulant in various regions of a metal foam heat exchanger. Particles with a higher residence time have a significant chance of being deposited in the metal foam structure. Although the Eulerian-Eulerian and Eulerian-Lagrangian models are widely deployed in a number of studies due to its convenience in simulating large-scale facilities, this method doesn't take into account the direct micromechanics and dynamics of particle displacements and velocities. Moreover, it doesn't account for particle-fluid (*i.e.* two-way coupling) and particle-particle (*i.e.* four-way coupling).

Several studies have harnessed a coupled Finite Volume Method & Discrete Element Method (CFD-DEM) to elucidate solid particle transport and its influence on the carrier fluid. There are two approaches to studying particle-fluid flow, namely unresolved and resolved CFD-DEM approach. The resolved

CFD-DEM approach is executed via a fictitious domain method or Immersed boundary method. This method is applicable if the DEM particle size exceeds the CFD mesh cell size. The opposite is true for the unresolved method. The resolved approach coupled with DEM method is extremely computationally demanding and only restricted to few particles. This approach is discussed in detail by Hager [7, 8]. Many of the existing CFD-DEM studies are based on unresolved method. Akbarzadeh and Hrymak [2] examined the influence of a sharp rectangular duct bend on the particle agglomeration patterns. Drag force is shown to be the primary driving force in initiating agglomeration at the duct bends. Afkhami *et al.* [1] studied turbulent channel flow using a coupled LES-DEM approach. The turbulent structure of the flow is largely responsible for amplifying particle-particle interactions.

Moreover, particle agglomeration was enhanced in high turbulence regions near the walls due to the shearing effect of the fluid flow. Mondal *et al.* [11] used resolved CFD-DEM to assess hydrodynamic bridging at narrow constrictions. The critical particle volume concentration largely depends on the outlet size, inlet size, and flow geometry. An increase in the particle-fluid density ratio and flow velocity increases the jamming probability (*i.e.* blockage). Interestingly, although the DEM particle size is larger than the CFD mesh cell size, both the unresolved and resolved method yielded identical results at low particle concentrations ($\phi = 5\%, 10\%, 15\%$). However, at $\phi = 20\%$, the unresolved method yielded inaccurate result due to the mesh cell size being equivalent to the inter-particle separation distance. There are very few studies that used the unresolved method for cases where the DEM particle size exceeds the CFD mesh size [3, 11]. To the best of the author's knowledge there is no concrete consensus among the research community about the applicability of the unresolved CFD-DEM in situations where the DEM particle size is significantly larger than the CFD mesh cell size.

The goal of this work is to conduct a preliminary investigation using the unresolved CFD-DEM methodology to examine particle-fluid flow and particle-deposition in 2D clear channels based on varying grid resolution.

Numerical Method and Computation Domain

Particle-laden Gas Flow Modelling

A coupled finite volume method & discrete element method numerical methodology is used in this investigation to account for isothermal particle-laden gas flow and particle deposition immersed in 2D clear channels. The equations that govern pore-level isothermal incompressible fluid transport [12] are:

$$\frac{\partial \varepsilon}{\partial t} + \nabla \cdot (\mathbf{u}_f \varepsilon) = 0, \quad (1)$$

$$\frac{\partial(\rho_f \epsilon u_f)}{\partial t} + \nabla \cdot (\rho_f \epsilon u_f u_f) = -\nabla p - F_{pf} \quad (2)$$

$$+ \nabla \cdot (\epsilon \tau) + \rho_f \epsilon,$$

where g is gravitational acceleration, u_f is the fluid velocity, ϵ is the void fraction within a CFD computation cell, F_{pf} is the volumetric particle-fluid interaction force, τ is the fluid viscous stress tensor, and ρ_f is the carrier fluid density [11]. The fluid in this study is assumed to be laminar and isothermal. The dominant forces in this study is the drag force and gravity force. Virtual mass force, Basset history force is neglected as the particle-fluid density ratio is significantly greater than one. Moreover, Brownian motion is neglected as submicron particles are not being considered. The equations that govern the solid particle translational motion are given as

$$m_i \frac{dV_i}{dt} \quad (3)$$

$$= m_i g + \sum_{j=1}^{k_i} (f_{cn,ij} + f_{dn,ij} + f_{ct,ij} + f_{dt,ij}) + f_{pf,i},$$

where V_i is the particle velocity, m_i is the particle mass, f_{cn} is the normal contact force between particles i and j , f_{dn} is the normal damping force, f_{ct} is the tangential contact force, f_{dt} is the tangential damping force, f_{pf} is the particle-fluid interaction force, and is given as

$$f_{pf,i} = f_{d,i} + f_{\nabla p,i} + f_{\nabla \cdot \tau,i} \quad (4)$$

Additionally, a cohesion model is incorporated into the DEM code. This model accounts for particle cohesiveness based on the particle surface energy density and is given by the following formulae [6]:

$$F_{C.E.D.} = \chi A_{contact} \quad (5)$$

In this study, the particles are assumed rigid, smooth, and isothermal. A *soft-sphere* discrete element method (DEM) based on a non-linear spring-slider-dashpot model [9] is used to model the discrete particulate phase. The DEM method can capture the particle-particle and particle-wall interactions (*four-way coupling*) unlike the Eulerian-Lagrangian method which assumes zero particle volume. The transient interaction between the carrier phase and discrete phase is enabled in order to capture the particle-fluid interaction (*two-way coupling*). To reduce the computational burden and the time taken to reach numerical convergence, a combined SIMPLE-PISO (*i.e.* PIMPLE) algorithm is deployed in the numerical studies presented herein. A generalized geometric-algebraic multi-grid (GAMG) solver and a Gauss-Seidel smoother is used to obtain the discretized pressure equations whilst a smoother symmetric Gauss-Seidel (sGS) is used to obtain the discretized velocity equations. Equation 3 is solved by an explicit time integration method. The DEM time-step is set at 10^{-6} s whilst a CFD (fluid) time-step is 10^{-4} s in order to comply with the Courant and Rayleigh number. The total simulation time is 1.10 s. A particle injection rate of 200 particles per second (pps) is enforced to achieve viable deposition process. Particles are injected from 0.20 s to 1.00 s. Particles are injected from the inlet. Particles start to inject from 0.20 s to ensure fluid flow has enough time to be fully developed from 0.00 s to 0.20 s. Sandstone particles of 2500 kg/m^3 is investigated. In order to achieve stable momentum-pressure coupling, the following values are assigned to the PIMPLE control: 2 non-orthogonal correctors, 2 correctors, and 20 non-

outer correctors. The PIMPLE algorithm is shown to achieve faster and stable numerical convergence than the standalone PISO algorithm.

Computational Domain and Boundary Conditions

The computation domain and dimensions of the clear channel is presented in figure 1.

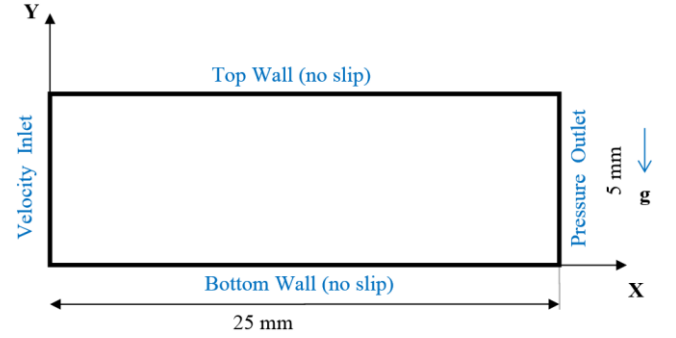


Figure 1. Computation domain of particle-laden air flow in clear channel.

The boundary conditions for the simulations are given in Table 1. An inlet velocity U_x of 0.50 m/s is assigned for all computational cases; a Reynolds number of 170 is registered. A no-slip boundary condition is enforced on the top and bottom wall. The carrier fluid is incompressible and isothermal air. Sandstone particles based on two different diameters is investigated: 350 μm and 500 μm .

	Velocity (m/s)	Pressure (Pa)
Inlet	0.5	Zero Gradient
Outlet	Zero Gradient	0
Top Wall	No Slip	Zero Gradient
Bottom Wall	No Slip	Zero Gradient

Table 1. Boundary conditions for the clear channel.

The simulations were carried out for 3 different computational grids: 88, 1000, 4000 cells. One grid consists of mesh cell size that are larger than the DEM particle size (*i.e.* 88 cells) which is the norm for the unresolved CFD-DEM method. Moreover, this method will be used to investigate the variation in numerical results when the CFD mesh cell size is smaller (*i.e.* 1000, 4000 cells) than the DEM particle diameter.

OpenFOAM software, a customizable C++ open-source CFD program, is used to simultaneously execute the particle solver (DEM) and fluid solver (FVM). The time-dependent variation of fouling layer and its effect on the pressure drop based on four various grids is investigated.

Results and Discussion

Particle deposition patterns for the 350 μm and 500 μm sandstone particles and fluid flow patterns based on three different grids are shown in figure 2 and figure 3 respectively. The computational grids are shown in the respective cases. The mesh cell size for grids 1 and 2 is larger than the DEM particle size. Whereas, the mesh cell size for grid 3 is smaller than the DEM particle size. Please note that the particles have been seeded at the same locations along the inlet plane for all grids and computation cases. The velocity contours depicting air flow and particle transport for the 6 cases is clearly illustrated. All snapshots were taken at the end of the simulation (*i.e.* $t = 1.10$ s); the simulations are transient meaning that particle deposition linearly increases with time from 0.20 s to 1.00 s. Maximum fluid velocity is realised around the mid-section of the clear channel connoting maximum sandstone deposit height. The particle deposition fraction, which is measured as a ratio of the total number of

particles deposited in the channel to the particle injection rate, is shown to be slightly lower for the 350 μm particles than the 500 μm particles. A summary of the results pertaining to the maximum fluid velocity, particle deposition fraction, numerical and analytical pressure drop is presented in table 2 and table 3 for the 350 μm and 500 μm sandstone particles.

Grid	Max Fluid Velocity [m/s]	Deposition Fraction [%]	Numerical Pressure Drop [Pa]	Analytical Pressure Drop [Pa]
1	0.800	60.50	0.265	0.250
2	0.790	59.00	0.271	0.255
3	0.850	44.00	0.321	0.319

Table 2. Summary of results for 350 μm sandstone particles.

The analytical pressure drop is obtained by the Ergun analytical equation [5] as shown in table 2 and table 3. Good agreement is observed between the numerical and analytical pressure drop. However, several studies have shown the Ergun equation (*i.e.* Darcy-Brinkman-Forchheimer equation) overestimates the pressure drop if the effective porosity is low [4, 14]. The average effective porosity for all cases in table 2 and table 3 is 92 % and 76 % respectively. In this study, it is found that the Ergun equation overestimates pressure drop values for all cases presented in table 3. However, introducing a correction factor of 0.1 lead to better agreement between the analytical and numerical pressure drop results. Likewise, a maximum discrepancy between the numerical and analytical value of only 6.8 % is realized for 500 μm particles as shown in table 3.

Both particles exhibit similar maximum particle velocities and maximum carrier fluid velocities. However, a major difference lies in the deposition fraction and pressure drop. A higher deposition fraction based on 500 μm sandstone particles is realised irrespective of computational grid except for Grid 2. The primary mechanism of transport for both particle types is gravitational sedimentation. The 500 μm particles settle to the bottom wall at a rapid pace than the 350 μm particles due to the higher inertia of the 500 μm particles. Therefore a high deposition fraction is encountered for the 500 μm case. Consequently, the higher deposition fraction yields a higher pressure drop. Moreover, a larger swathe of 500 μm deposit is located between the inlet and the midsection channel unlike the 350 μm deposit.

Grid	Max Fluid Velocity [m/s]	Deposition Fraction [%]	Numerical Pressure Drop [Pa]	Analytical Pressure Drop [Pa]
1	1.110	61.50	0.788	0.797
2	1.110	57.00	0.757	0.712
3	1.000	63.00	0.746	0.698

Table 3. Summary of results for 500 μm sandstone particles.

As shown in figure 3, the 500 μm particles show no significant deviation in the deposition fraction and pressure drop for all 3 grids. However, the deposit layer for grid 3 is uniform throughout the channel. According to table 3, there is a negligible difference in the maximum fluid velocity. The same observation is realised for the 350 μm particles (table 2) with the exception of grid 3. A strong deviation to the fluid trajectory due to the heavy presence of 500 μm particles (*i.e.* retro-action) is realised for all 3 grids. The current literature on CFD-DEM studies claim that the use of unresolved method may lead to inaccurate results in the event the DEM particle diameter greatly exceeds the mesh cell size. In other words, the mesh cell size must be larger (*i.e.* at least three to four times larger than DEM particle diameter) than the particle diameter (*i.e.* grids 1 & 2) which is the standard protocol for any

unresolved CFD-DEM simulations. However, the results presented in figures 2, 3, and 4 display a very interesting observation. For instance, the particle distribution along the streamwise direction in grid 3 (where the DEM particle diameter exceeds the CFD mesh cell size) is sensibly similar to the particle distribution patterns in grid 1 and grid 2. Secondly, the maximum difference in the deposition fraction for the 500 μm particles is 10.5 %. As far as the authors' are aware, only two studies [3,11] showed that the unresolved method can yield accurate results in only a few cases. The increase in accuracy was achieved by incorporating a void fraction (*i.e.* 'big particle') method or a smoothing model which smoothens the exchange fields between the gas and solid void fraction. However, the authors enunciated that such sub-models deployed within the unresolved approach improve the accuracy in only a few cases. This is attributable to the misinterpretation of the DEM particle's volume depending on the discretization of the domain. Although these sub-models have not been explicitly deployed in OpenFOAM, the deposition characteristics are very similar in all four grids (figures 2,3,4). Interestingly, although the quantitative results (*i.e.* table 3 and table 4) and the particle deposition patterns are similar among all four grids, there exist subtle differences in the smoothness of the exchange fields between the gas and solid void fraction depicted by the yellow arrows as shown in figure 5.

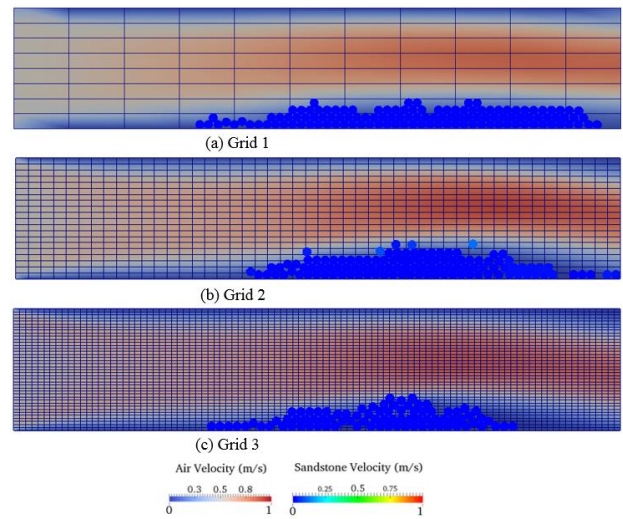


Figure 2. Contour plots for 350 μm , $U_\infty = 0.50$ m/s. Direction of flow from left to right.

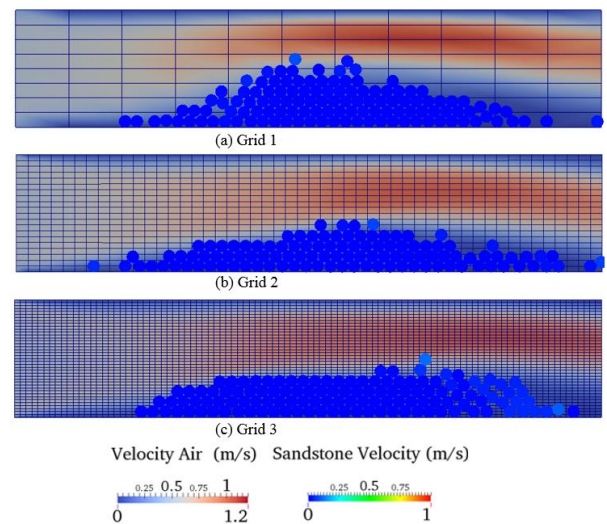


Figure 3. Velocity contour plots for 500 μm particles, $U_\infty = 0.50$ m/s. Direction of flow from left to right.

Cells without any DEM particles correspond to a gas fraction of 100 %. The presented numerical model is capable of computing the particle and fluid displacements and velocities with near identical results for all grids albeit a slight misinterpretation in the gas void fraction due to the absence of a void fraction model.

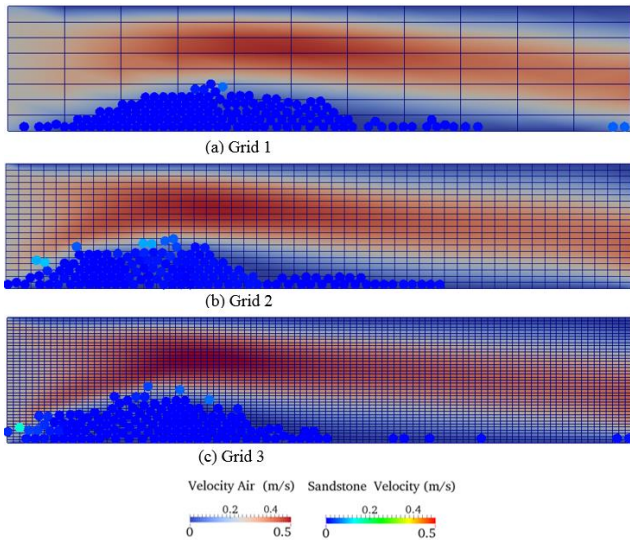


Figure 4. Velocity contour plots for 350 μm particles at $t = 1.10$ s, $U_\infty = 0.25$ m/s. Direction of flow from left to right.

Particle deposition fraction is near identical in all cases. This is also attributable to the fact that particle motion is largely influenced by Newton's second law rather than grid resolution due to the high particle mass in confined channels. The numerical method presented herein could be deployed even if a CFD mesh cell size exceeds the DEM particle size without a void fraction model as the results are similar irrespective of the grid resolution. But the method leads to a rough representation of the gas phase fraction as shown in grid 3 in figure 5.

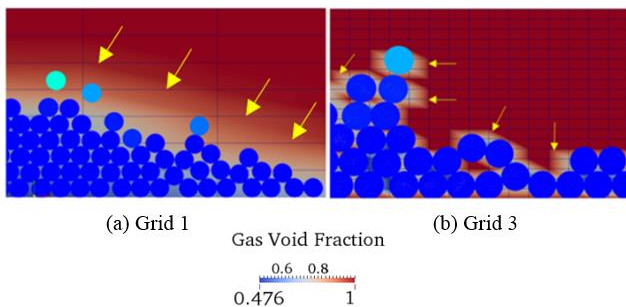


Figure 5. Close-up of the gas void fraction for 350 μm particles at $t = 1.00$ s, $U_\infty = 0.25$ m/s. Direction of flow from left to right.

Conclusions

This preliminary numerical study investigates particle-laden gas flow and particle deposition in a clear channel. This is achieved by developing and implementing a coupled finite volume and discrete element method in OpenFOAM namely the unresolved CFD-DEM approach. The primary mode of transport for the sandstone particles is gravitational sedimentation. A significant reduction in the CFD mesh cell size showed minuscule difference in the fluid patterns, particle deposition patterns, and pressure drop. However, the smoothness between the gas and solid fraction is reduced. The next step will involve a more detailed comparative analysis between the unresolved and resolved CFD-DEM approach coupled with experimental validation.

References

- [1] Afkhami, M., Hassanpour, A., Fairweather, M. & Njobuenwu, D. O., Fully coupled LES-DEM of particle interaction and agglomeration in a turbulent channel flow, *Computers and Chemical Engineering*, **78**, 2015, 24-38.
- [2] Akbarzadeh, V. & Hrymak, A., Coupled CFD-DEM of particle-laden flows in a turning flow with a moving wall. *Computers & Chemical Engineering*, **86**, 2016, 184-191.
- [3] Bagherzadeh, M., *Modelling Single Particle Settlement by CFD-DEM Coupling Method*. Thesis. Department of Transport and Planning, TU Delft University, 2014.
- [4] Bear, J. *Dynamics of fluids in porous media* New York, Dover, 1988.
- [5] Ergun, S., Fluid flow through packed columns, *Chemical Engineering Progress*, **48**, 1952.
- [6] Fernandez, X. R. & Nirschl, H., Simulation of particles and sediment behaviour in centrifugal field by coupling CFD and DEM, *Chemical Engineering Science*, **94**, 2013, 7-19.
- [7] Hager, A., *CFD-DEM on Multiple Scales. An Extensive Investigation of Particle-Fluid Interactions*. PhD Thesis. Johannes Kepler Universitat Linz, 2014.
- [8] Hager, A., Kloss, C., Pirker, S. & Goniva, C., Parallel Open Source CFD-DEM for Resolved Particle-Fluid Interaction, *J. Energy and Power Engineering*, **7**, 2013, 1705-1712.
- [9] Johnson, K.L., *Contact Mechanics*. Cambridge: Cambridge University Press, 1987.
- [10] Lakeh, K. S., Martinelli, A., Torre, A. D. L., Montenegro, G. & Onorati, A., Numerical study of compressor fouling mechanism based on Eulerian-Eulerian approach, *Energy Procedia*, **82**, 2015, 258-264.
- [11] Mondal, S., Wu, C. & Sharma, M. M., Coupled CFD-DEM simulation of hydrodynamic bridging at constrictions. *International Journal of Multiphase Flow*, **84**, 2016, 245-263.
- [12] Narsilio, G., Buzzi, O., Fityus, S., Yun, S. & Smith, D., Upscaling of Navier-Stokes equations in porous media: Theoretical, numerical and experimental approach, *Computers and Geotechnics*, **36**, 2009, 1200-1206.
- [13] Sauret, E. & Hooman, K., Particle size distribution effects on preferential deposition areas in metal foam wrapped tube bundle. *Int. J. of Heat and Mass Transfer*, **79**, 2014, 905-915.
- [14] Sivanesapillai, R., Steeb, H. & Hartmaier, A., Transition of effective hydraulic properties from low to high Reynolds number flow in porous media, *Geo. Research Letters*, **41**, 4920-4928.
- [15] Tryggvason, G., Virtual motion of real particles. *Journal of Fluid Mechanics*, **650**, 2010, 1-4.
- [16] Zhou, L., Two-phase turbulence models in Eulerian-Eulerian simulation of gas-particle flows and coal combustion, *Procedia Engineering*, **102**, 2015, 1677-1696.